Hydrol. Earth Syst. Sci. Discuss., 6, 1233–1260, 2009
www.hydrol-earth-syst-sci-discuss.net/6/1233/2009/

Hydrology and Earth System Sciences Discussions

Papers published in *Hydrology and Earth System Sciences Discussions* are under open-access review for the journal *Hydrology and Earth System Sciences*

Application of satellite microwave remote sensed brightness temperature in the regional soil moisture simulation

X. K. Shi, J. Wen, L. Wang, T. T. Zhang, H. Tian, X. Wang, R. Liu, and J. H. Zhang

Laboratory for Climate Environment and Disasters of Western China, Cold and Arid Regions Environmental and Engineering Research Institute, Chinese Academy of Sciences, Lanzhou, Gansu, China

Received: 15 January 2009 – Accepted: 20 January 2009 – Published: 26 February 2009

Correspondence to: J. Wen (jwen@lzb.ac.cn)

Published by Copernicus Publications on behalf of the European Geosciences Union.

Abstract

As the satellite microwave remote sensed brightness temperature is sensitive to land surface soil moisture (SM) and SM is a basic output variable in model simulation, it is of great significance to use the brightness temperature data to improve SM numerical simulation. In this paper, the theory developed by Yan et al. (2004) about the relationship between satellite microwave remote sensing polarization index and SM was used to estimate the land surface SM from AMSR-E (Advanced Microwave Scanning Radiometer – Earth Observing System) brightness temperature data. With consideration of land surface soil texture, surface roughness, vegetation optical thickness, and the AMSR-E monthly SM products, the regional daily land surface SM was estimated over the eastern part of the Qinghai-Tibet Plateau. The results show that the estimated SM is lower than the ground measurements and the NCEP (American National Centers for Environmental Prediction) reanalysis data at the Maqu Station (33.85° N, 102.57° E) and the Tanglha Station (33.07° N, 91.94° E), but its regional distribution is reasonable and somewhat better than that from the daily AMSR-E SM product, and its temporal variation shows a quick response to the ground daily precipitations. Furthermore, in order to improve the simulating ability of the WRF (Weather Research and Forecasting) model to land surface SM, the estimated SM was assimilated into the Noah land surface model by the Newtonian relaxation (NR) method. The results indicate that, by fine tuning of the quality factor in NR method, the simulated SM values are improved most in desert area, followed by grassland, shrub and grass mixed zone. At temporal scale, Root Mean Square Error (RMSE) values between simulated and observed SM are decreased 0.03 and 0.07 m^3/m^3 by using the NR method in the Maqu Station and the Tanglha Station, respectively.

1 Introduction

Soil moisture (SM) is an important factor in global water and energy cycles. It controls the partition between the sensible and latent heat fluxes (Prigent et al., 2005) and the redistribution of rainfall into infiltration, surface runoff and evaporation on the earth surface (Delworth and Manabe, 1988; Vinnikov and Yeserkepova, 1991; Wagner et al., 2003), and thus influences the climate change by land-atmosphere interaction in the near surface layer (Clark and Arritt, 1995; Gallus and Segal, 2000; Lanicci et al., 1987). As a result, it is crucial to get an accurate SM field to improve the simulations in the land surface model or the weather/climate model which couples a land surface model.

Traditionally, there are two ways to get SM data. First, some operational networks of in situ soil moisture sensors have been established and maintained to provide long-term soil moisture measurements, such as the Soil Climate Analysis Network and the Oklahoma Mesonet, etc. These networks provide valuable distributed point measurements but are insufficient to characterize the spatial and temporal variability of SM at large scales (Njoku et al., 2003). Second, the numerical model products combined with ground observations form the low-resolution reanalysis SM datasets, such as the reanalysis datasets from American National Centers for Environmental Prediction (NCEP) or European Centre for Medium-range Weather Forecast (ECMWF), etc. These datasets usually have low spatial resolution and can be used as model background fields.

Nowadays, the satellite remote sensing observations provide an integrated global SM monitoring capability and work as an effective way to overcome the shortages of the traditional ways. Compared to the early developed optical remote sensors, which are sensitive to land surface reflectance and land surface temperature, the newly developed satellite microwave sensors show a great advantage in estimate of land surface SM. As a fact, the dielectric constants of water and dry soil are 80 and 3, respectively, different SM values make the dielectric constant of soil vary, and hence change the emissivity of soil (Hallikainen et al., 1985). Furthermore, the satellite passive mi-

crowave radiometers can work in all weather conditions regardless the cloud condition. It also can penetrate vegetation and surface topsoil to some extent. With the launch of Scanning Multichannel Microwave Radiometer (SMMR) aboard Seasat and Nimbus-7 in 1978 and later other microwave radiometers, such as Special Sensor Microwave/Imager (SSM/I) and Tropical Rainfall Measuring Mission/Microwave Imager (TRMM/TMI), the satellite microwave remote sensing radiometers have greatly accelerated the process of SM retrieval at regional scale (Gao et al., 2006; Vinnikov et al., 1999; Wen et al., 2005). Especially, the AMSR-E (Advanced Microwave Scanning Radiometer – Earth Observation System) aboard the Aqua satellite launched on 4 May 2002 measures radiation at six frequencies in the range 6.9–89 GHz, all dual polarized. Compared to the SSM/I, AMSR-E's 6.9 GHz and 10.6 GHz channels have much longer wavelengths, which have better penetration ability and are more sensitive to the change of dielectric constant of soil. Simonetta et al. (2006) estimated the SM from AMSR-E observations by applying a simple radiation transfer model. McCabe et al. (2005a, b) also estimated the SM from AMSR-E by a single frequency channel radiation transfer model and then discussed the impact of vegetation on SM calculation.

In order to apply the SM estimated from satellite remote sensing into the numerical simulations, it is common to use the data assimilation method. Firstly, the estimated SM includes some errors resulting from some uncertainties, such as the soil type, surface roughness and vegetation coverage, etc. It is also limited by satellite scanning time. Therefore, the data can not be applied as the model background fields solely. Secondly, the SM information can be easily reached by simulations of land surface models, but it is too sensitive to the model structure and model parameters. Wei (1995) pointed out that the operational SM product can be estimated by combining both satellite SM and numerical simulated SM. With the process of assimilation, the consequent SM datasets have higher spatial-time resolution and smaller errors than those solely using satellite data or numerical simulations. Huang et al. (2007) confirmed that the assimilation procedure could improve the SM estimation significantly. In general, the commonly used methods of assimilation are four-dimensional variational method, Kalman filter

method, and ensemble Kalman filter method, etc. They could yield good precision, however, they need a longer computation time than the general interpolation methods.

To retrieval the SM from satellite brightness temperature data and to assimilate this SM into numerical simulations are two key procedures for using satellite brightness temperature data to improve model simulation of SM, and they are generally done separately in previous researches. In this paper, the regional SM datasets are estimated from AMSR-E based on the relationship between satellite microwave remote sensing polarization index and SM proposed by Yan et al. (2004). Next, the estimated SM is assimilated into the Noah land surface model in the WRF (Weather Research and Forecasting) model through the four-dimensional Newtonian relaxation (NR) method (Hoke and Anthes, 1976). With considering all these aspects, the objective of this paper is to provide a simple approach to apply satellite microwave remote sensed brightness temperature data into the WRF model for improving the regional simulation of SM.

Firstly, brief descriptions about the geophysical and meteorological characteristics of study area and the satellite remote sensing data are given in Sect. 2 after the introduction in this investigation. Secondly, an algorithm developed by Yan et al. (2004) is introduced for SM estimates from the AMSR-E. And then, a four-dimensional NR method for assimilating SM into the Noah land surface model is designed. In Sect. 4, the regional estimated SM values are validated by using ground measurements. The inter-comparings among the simulated SM values with assimilation procedure, non-assimilation procedure and directly insertion procedure which directly replace the model background field of SM with the estimated SM datasets are presented in Sect. 5. The main conclusions and discussions are made in the last section.

2 Descriptions of the study area and the datasets

An eastern part of the Qinghai-Tibet Plateau which has high average altitude and typical continental plateau climate is selected as the study area (Fig. 1a). Its harsh environment keeps human activity away and results in few of ground meteorology obser-

vations. It is known that the thermal dynamics of this plateau has significant impact on the Eastern Asian monsoon and global weather/climate system (Wu et al., 2005). If the satellite remote sensing data are used in land surface SM simulation in this area, the mechanism research of thermal dynamics effect on weather/climate variability in such an inaccessible but important area will be improved.

Figure 1b shows the land use classification of the study area which is the domain of WRF simulation in this investigation. There are Qaidam basin desert and Kumtag desert on the northwest, Tengger desert on the northeast, and shrub and grass mixed areas surround the deserts. On the southeast part, it is mostly grassland with several lakes sparsely distributed. Among these lakes, Lake Qinghai, Lake Gyaring and Lake Ngoring are the bigger three.

The ground measurement datasets deployed in this study are taken at two sites. The first one is an ECH2O SM meter installed at the Maqu (33.85° N, 102.57° E), where is the water source region of the Yellow River, no precipitation observations are available at this site. The second site is located at the Tanglha (33.07° N, 91.94° E), which is a boundary layer meteorology observation station near the Qinghai-Tibet railway. There are precipitation observations at this site. Both sites have 5 cm depth SM measurements. These observation datasets will be used to validate the estimated SM from AMSR-E and the simulated SM from WRF model.

The satellite brightness temperature data deployed in this investigation are the AMSR-E L2A re-sampled product which spatial resolution is 12 km (the detail information about this product is available on http://nsidc.org/data/amsre/index.html). AMSR-E radiometer scans the study area 2 times per day, and the ascending orbital observations covered July 2008 at about 14:00 Beijing Standard Time (BST) are only used in this research.

The land surface model used in SM simulation is the Noah land surface model based on the one developed in the Oregon State University (Chen and Dudhia, 2001) and coupled into the WRF model. The Noah land surface model calculates the SM values in four layers of 10 cm, 30 cm, 60 cm and 100 cm. After year 2005, the NCEP 1°×1°

reanalysis dataset consists of four SM layers, 0–10 cm, 10–40 cm, 40–100 cm and 100–200 cm. Because the NCEP SM values are not interpolated to the depth of soil layers for the Noah land surface model and are usually used as model background fields directly in simulations, the SM estimated from the AMSR-E will be also used directly in the simulations of top layer SM in the Noah land surface model.

3 Methodology

3.1 Soil moisture estimates from satellite microwave remote sensing data

Because of the large difference between the dielectric constants of dry soil and water as mentioned previously, the soil emissivity mainly depends on the SM. The complex dielectric constant ε of soil can be represented as (Hallikainen et al., 1985)

$$\varepsilon = (a_0 + a_1 S + a_2 C) + (b_0 + b_1 S + b_2 C) m_v + (c_0 + c_1 S + c_2 C) m_v^2, \quad (1)$$

where S and C are sand and clay components of the soil layer, respectively, which are the physical property of soil layer, m_v is volumetric SM, and a_0, a_1, a_2, b_0, b_1, b_2, c_0, c_1 and c_2 are empirical coefficients listed in Table 1.

Assuming a smooth soil surface and omitting bulk scattering, the microwave reflection indexes of horizontal and vertical components of the soil surface (r_H, r_V) can be calculated with the Fresnel equation (Jackson et al., 2002; Ulaby et al., 1981)

$$r_H = \left| \frac{u\cos\theta - \sqrt{u\varepsilon - \sin^2\theta}}{u\cos\theta + \sqrt{u\varepsilon - \sin^2\theta}} \right|^2, \quad (2)$$

$$r_V = \left| \frac{\varepsilon\cos\theta - \sqrt{u\varepsilon - \sin^2\theta}}{\varepsilon\cos\theta + \sqrt{u\varepsilon - \sin^2\theta}} \right|^2, \quad (3)$$

where θ is the incidence angle, u is the relative magnetic susceptibility, which is 1.0 for non-magnetic materials.

When the land surface roughness is taken into account, the microwave reflection indexes of the horizontal and vertical components (R_H, R_V) will be modified as

$$R_H = [(1 - Q) r_V + Q r_H] e^{-h}, \quad (4)$$

$$R_V = [(1 - Q) r_H + Q r_V] e^{-h}, \quad (5)$$

where Q and h are the polarization ratio and the surface roughness parameter, respectively. In general, $0 \le Q < 0.5$, $Q = 0.174$ is taken in this investigation (Njoku and Chan, 2006).

The vector radiative transfer (VRT) equation for a uniform atmospheric layer and land surface with vegetation can be written as (Jin, 1998)

$$T_{BP} = (1 - R_P) e^{-\tau} T_s + (1 - e^{-\tau})(1 + R_P e^{\tau}) T_a, \quad (6)$$

where T_{BP} is brightness temperature, p is either vertical (V) or horizontal (H) polarization, τ is the total opacity of atmospheric layer and vegetation layer, R_P is the polarized reflection index from Eq. (4) and/or Eq. (5), T_a and T_s are the average physical temperatures of the uniform atmospheric layer and land surface, respectively. As T_a is generally smaller than T_s, it can be rewritten as $T_a = (1 - \delta_T) T_s$ with $0 \le \delta_T \le 1$, δ_T is called as the air temperature parameter. In Eq. (6), the reflection of the top layer vegetation and the scattering of the vegetation layer are ignored.

It is commonly use the microwave polarization difference index (MPDI) to characterize the brightness temperature difference between vertical and horizontal channels. From Eq. (6), the MPDI can be rewritten as

$$\mathrm{MPDI} = \frac{T_{BV} - T_{BH}}{T_{BV} + T_{BH}} = \frac{(R_H - R_V) e^{-2\tau} [1 + \delta_T (e^{\tau} - 1)]}{2 - (R_H + R_V) e^{-2\tau} - \delta_T (1 - e^{\tau}) [2 + (R_H + R_V) e^{-\tau}]}. \quad (7)$$

By pluging Eqs. (4) and (5) into (7), the MPDI can be simplified as

$$\mathrm{MPDI} \approx \frac{(R_H + R_V)(1-2Q)(1+\delta_T)}{2e^{2\tau}e^{h}(1-\delta_T)-(R_H-R_V)}. \tag{8}$$

The MPDI expressed in Eq. (8) clearly reveals its dependence on the SM, the surface roughness parameter h, the atmospheric and vegetation opacity τ and the air temperature parameter δ_T. For example, the increasing of either h, τ, Q, or $(1-\delta_T)$ diminishes the difference of surface polarization radiations and hence decreases MPDI. On the other hand, the increasing of the SM boosts (R_H+R_V) much more than (R_H-R_V), therefore it yields a bigger radiation difference and MPDI value. As seen in previous equations, (R_H+R_V) and (R_H-R_V) are functions of m_v and will be noted as R_+ and R_- for simplicity.

Statistically, parameters τ, Q, h, and δ_T of the same region in the same month should change little, so the variation of the MPDI will embody the change of the SM (Yan and Jin, 2004). With Eq. (8), there is

$$\frac{\mathrm{MPDI}}{\langle\mathrm{MPDI}\rangle} \approx \frac{2e^{2\tau}e^{h}(1-\delta_T) - R_+(\langle m_v\rangle)}{2e^{2\tau}e^{h}(1-\delta_T) - R_+(m_v)} \equiv \frac{a - R_+(\langle m_v\rangle)}{a - R_+(m_v)}, \tag{9}$$

where $a=2e^{2\tau}e^{h}(1-\delta_T)$, $\langle\mathrm{MPDI}\rangle$ is the monthly average of MPDI and $\langle m_v\rangle$ is the monthly average of m_v. Given a, $\langle\mathrm{MPDI}\rangle$ and $\langle m_v\rangle$, the $R_+(m_v)$ can be derived from the current observation of MPDI, and then the m_v can be found out by iteration.

As for the parameter a, Yan et al. (2004) treated it as constant, which is solved from two sets of known MPDI and m_v at different time. In our case, it is impossible to have two observations of any one grid point in advance. Therefore τ and h are calculated based on previous algorithms (Meesters et al., 2005; Wang et al., 2006) in this paper.

The above scheme takes into account of the impact of soil type, surface roughness, and vegetation optical thickness in SM estimates. However, a key prerequisite is knowing the monthly average SM ($\langle m_v\rangle$), which is not an easy task considering that there are only very limited records available for the whole Qinghai-Tibet Plateau. In order to

provide the monthly average SM for each grid point in the simulation area, we use the AMSR-E global monthly SM product (resolution 1°×1°) as the $\langle m_v\rangle$, and re-sampling it and the AMSR-E brightness temperature data to the 10 km resolution of the model grids for further processing.

3.2 Newtonian relaxation assimilation scheme

The SM estimated from AMSR-E is assimilated into the Noah land surface model coupled in the WRF model by the Newtonian relaxation (NR) assimilation scheme in this investigation. The idea of this method is with adding a fake tendency term, proportional to the difference between a simulated value and the observed value, into one or several prediction (or forecast) equations to make the simulated value close to real observation and make all variables balanced by model dynamical framework in the entire nudging time. This nudging method can effectively damp the inertia-gravity wave generated by new data insertion. The NR result can be used as an initial field of forecast to improve the accuracy of prediction. Furthermore, multiple time observations can be inserted into this initial field optimization process, and this will raise the effective resolution of observations (Hoke and Anthes, 1976; Kistler, 1974).

The SM in the Noah land surface model is simulated through the application of the diffusivity form of Richards equation, which can be formulated as follows:

$$\frac{\partial m_v}{\partial t} = \frac{\partial}{\partial z}\left(D(m_v)\frac{\partial m_v}{\partial z}\right) + \frac{\partial K(m_v)}{\partial z} + S(m_v), \tag{10}$$

where K(m/s) is the hydraulic conductivity, D(m^2/s) is the soil water diffusivity, S(m^3/m^3 s) is representative for sinks and sources (i.e. rainfall, dew, evaporation and transpiration), t(s) represents the time, and m_v is the soil moisture. The non-linear $K-m_v$ and $D-m_v$ relationship are defined by the formulation of Cosby et al. (1984) for 9 different soil types.

By adding a relaxation term on the right hand of Eq. (10), the assimilation equation

reads

$$\frac{\partial m_v}{\partial t} = \frac{\partial}{\partial z}\left(D(m_v)\frac{\partial m_v}{\partial z}\right) + \frac{\partial K(m_v)}{\partial z} + S(m_v) + G\omega(x,y,1,t)\varepsilon(x,y,1)(m_v^o - m_v), \quad (11)$$

where G denotes the strength of the relaxation, which determines the relative value of the assimilation term with respect to all other physical forcing terms in Eq. (11). G has dimension of s^{-1}, and it has to be adjusted accordingly to match the slowest physical process in this equation. A prerequisite of G is to satisfy the stability criterion $G \leq 1/\Delta t$, where Δt is the nudging time of the analytical field. Generally, the simulation results are too close to observations and thus breaks the harmonious of the fields if G is too big, or, the assimilation data plays no role in simulation if G is too small. Empirically, G varies in range 10^{-5}–$10^{-3}\,s^{-1}$ and is usually set as $10^{-4}\,s^{-1}$. $\omega(x,y,1,t)$ is the four-dimensional assimilation weighting function. $\varepsilon(x,y,1)$ is the quality factor of analytical value, which is in range 0–1.0 and relies on the data quality and distribution. m_v° is the grid observation value by interpolating observations of neighbor times. In this research, only the first layer SM is assimilated into the Noah land surface model. More details setting about G, ω and ε are also explained in Sect. 5. The nudging time for every observation data is 6 h in this study.

4 Analysis of the soil moisture estimated from AMSR-E

4.1 Evaluation of the estimated soil moisture

In this section, the estimated SM is validated by using the ground observations on 7 July 2008. In addition, no precipitation event occurred in this area during the study period, this circumstance is favorable to link the regional distribution of SM to the land use classification, and it is also suitable for inter-comparing between SM values from different sources. In addition, the average SM of monthly AMSR-E SM products of July in 2000–2007 was taken as the monthly average SM of July 2008, due to lack of the monthly AMSR-E SM product at that time.

Figure 2a presents the regional distribution of the estimated SM which original spatial resolution is about 12 km. The regional distributions of daily AMSR-E SM product and NCEP SM are also provided (Fig. 2b and Fig. 2c) for inter-comparing purpose. The estimated SM values in the desert areas are ranged 0.06–0.08 m^3/m^3 and indicate a good correspondence to the distributions between the estimated SM and the land use classification. In shrub and grass mixed areas, the estimated SM values are ranged 0.04–0.08 m^3/m^3, which are slightly smaller than actual observations. The estimated SM values are about 0.08–0.22 m^3/m^3 in the grasslands and reach maximum in the Songpan grassland (32.00–34.00° N, 102.00–104.00° E), Sichuan province. A conclusion has been drawn that the regional distribution of the SM estimated from AMSR-E is acceptable.

Figure 2b presents the regional distribution of the daily AMSR-E SM product which original spatial resolution is 25 km. The regional distribution pattern of the SM product is similar to that of the estimated SM in both the general tendency and the numerical values for each land use classification. The main differences between them are embodied in the SM distribution of the desert in the northwest and the SM values of the grassland in the southeast. This product gives SM values ranged 0.06–0.10 m^3/m^3 for the northwest desert area, and the distribution of this SM product deviates from the distribution of desert. In grassland, the SM values are slightly larger than the estimated SM values and their distributions agree better to the distribution of grassland. However, another disadvantage of the product is that the SM retrieval is not available for the Songpan grassland where there is a large area of high SM values. In general, the SM differences between the grassland and the desert in the SM product are smaller than that in the estimated SM.

Figure 2c is the regional distribution of the NCEP SM which original spatial resolution is 1°×1°. This product is the SM background field in simulation of the Noah land surface model in this paper. Basically this product represents the characteristic of SM distribution in both desert and grassland. However, the SM values in desert, 0.10–0.20 m^3/m^3, are obviously too high. The SM values in shrub and grass mixed area and grassland

are 0.20–0.25 m^3/m^3 and 0.25–0.30 m^3/m^3, respectively. Compared with the estimated SM, this product does not provide accurate information in shrub and grass mixed area, and misses the maximal SM area in the Songpan grassland due to its low resolution, either.

4.2 Validation of the estimated soil moisture

Before assimilating the estimated SM into the Noah land surface model for simulation, the estimated SM is validated by using the 5 cm depth SM data collected in July 2008 at both the Maqu Station and the Tanglha Station. The results are shown in Fig. 3.

The land surface type of the Maqu Station is grassland with a 3512 m altitude. As shown in Fig. 3a, the temporal variations of the estimated SM and the NCEP SM are highly coincidence with the SM measured at this ground station. Especially, three decreasing period of SM in 1–10, 14–20 and 21–30 July are all evidently shown. As for the data value, NCEP SM is closer to the ground observations than the SM estimated from AMSR-E. However, the estimated SM provides better evaluation of the low SM values than that of the NCEP SM. A small amplitude of the NCEP SM, compared to the ground measurements, is another disadvantage.

The land surface type of the Tanglha Station is grassland with a 5100 m altitude. As shown in Fig. 3b, the temporal variations of the estimated SM, the NCEP SM and the ground observations have similar trend. The NCEP SM provides much higher values than the ground observations, while the SM estimated from AMSR-E yields lower values than the ground observations. Furthermore, the estimated SM has smaller relative error compared to the NCEP SM. Gruhier (2008) pointed out that, the daily AMSR-E SM product is not able to capture absolute SM values at current stage, but it provides reliable information on land surface SM temporal variability, at seasonal and rainy event scale. By analyzing the precipitation of July in the Tanglha Station, the estimated SM presents a good correspondence of SM variation and rainy events. For example, after rainy events of 14, 24 and 30 July, the estimated SM reveals more clearly increasing

trend compared to the NCEP SM.

Based on previous comparison, the estimated SM is smaller than the ground observations. A possible reason is that the monthly average SM resulted from the monthly AMSR-E SM product at July is not accurate enough though several other factors have been considered, such as the soil type, surface roughness and vegetation optical thickness. Therefore, an accurate monthly average SM is essential for the way to better estimate SM in this investigation. Fortunately, the Soil Moisture and Ocean Salinity Mission (SMOS, more information in http://smsc.cnes.fr/SMOS/) has been scheduled for launch on April 2009, which is equipped with L-band (1.4 GHz) passive microwave radiometer. This radiometer is much sensitivity to the land surface SM and could provide more precise monthly SM values.

5 Assimilating the estimated soil moisture to the simulations of WRF

The accuracy of a numerical model simulation or forecasting is influenced not only by the model matureness, but also by the quality of initial variable fields. In this section, the NR method is deployed to assimilate the SM estimated from AMSR-E to the Noah land surface model in the WRF model, and then the regional and temporal patterns of simulated SM will be analyzed in this section.

5.1 Regional distribution of the simulated soil moisture

From the analysis in Sect. 4, it is found that the estimated SM and the NCEP SM have same temporal trend, but have different values in the regional distribution. These evident differences are mainly reflected in: (1) NCEP SM values are high in desert area; (2) AMSR-E derived SM values are low in shrub and grass mixed zone. So, the quality factor in NR method is simply set according to the land use category, instead of 1.0 as usually setting. The best way to set the quality factor is to use the statistical errors between actual SM values and estimated SM values. However, these statistical

errors can't be achieved in a short period for lacking of actual SM measurements in the Qinghai-Tibet Plateau. So, if the land use category isn't desert and the estimated SM less than 0.05 m^3/m^3, then the quality factor is set to 0.5 at this grid, If the land use category isn't desert and the estimated SM is greater than 0.05 m^3/m^3 and less than 0.1 m^3/m^3, then the quality factor is set to 0.8 at this grid. The quality factor is set to 1.0 for other cases. The relaxing strength factor is set to 0.00037 s^{-1} at all grids, and this setting could bring the best simulation results which are close to ground observations.

In this paper, three nested domains are used in the WRF model for simulating the SM distribution. Among these three domains, the third one which is the smallest one has the highest resolution of a 10 km grid spacing. In the third domain, the WRF model could provide more detail atmospheric force fields and land use category for the Noah land surface model, and similarly, the Noah land surface model could produce better water and heat fields to fed to the WRF model as the bottom boundary conditions. The estimated SM is assimilated in the third area only. Because there are few ground observation stations in this study area, it is hard to verify which method could yield better SM development, so the estimated SM at 7 July 14:00 BST is selected again to do assimilation test, and the simulation result can be verified by the land use category. The entire simulating period spans from 02:00 to 14:00 BST 7 July, when the period of 02:00–08:00 BST is taken as the model spin-up time and the model get harmonious atmospheric and land surface fields at 08:00 BST, the period of 08:00–14:00 BST is model assimilation period.

Figure 4 is the simulated regional distribution of SM in assimilated test and none assimilated test, it is found that the simulated SM values in assimilated test decrease in almost the entire study area. The changes of SM values between assimilated test and none assimilated test in desert area and shrub/grass mixed zone are ranged −0.02–(−0.04) m^3/m^3 and −0.04–(−0.06) m^3/m^3, respectively. In assimilation test, the simulated desert SM values in Qaidam basin, which locates in the north Qinghai-Tibet Plateau, are ranged 0.1–0.15 m^3/m^3 and have a better agreement with the distribution of desert area than the result in none assimilated test. This situation also happens in

the Tengger desert. In the southern Qinghai province (95–97° E, 31–33° N), simulated SM values in assimilated test obviously decrease with good corresponding to a small bare ground tundra zone. In the southwestern Qinghai province (90–93° E, 31–34° N), simulated SM values also obviously decrease in small shrub and grass mixed zone. In addition, the simulated SM values in assimilated test have almost no change if the estimated SM values are absence.

In summary, it can be concluded that after assimilating by using the NR method, the regional distribution of simulated SM is improved most in desert area, followed by grass, shrub and grass mixed zone.

5.2 Temporal variation of the simulated soil moisture

In the sense of temporal scale, the objective of the assimilation procedure is to syncretize the variation of estimated SM to the SM background field of numerical model, and make the simulated SM values approach to ground observations for improving the long term's simulating result of numerical model.

In this section, three tests are designed to check the influence of assimilation methods for the numerical simulations. The first test uses the Newtonian relaxation method (NR), the second test uses the direct insertion method (DI), and the third test doesn't take any assimilation step (NO), then the simulated results are validated by the data collected from the Maqu Station and the Tanglha Station, as shown in Fig. 5. The assimilation and simulation parameters in these three tests are set as that described in Sect. 5.1, the simulation period spans 14 days from 14:00 BST on 17 July to 14:00 BST on 31 July, the lateral boundary condition is updated every 6 h, same as the output frequency of the simulation results. The assimilating period is from 08:00 to 14:00 BST for NR method each day, and at 14:00 BST for DI method each day. In addition, the Root Mean Square Error (RMSE) is used to evaluate the simulation results. It defines

as follows:

$$\mathrm{RMSE}=\sqrt{\frac{1}{N}\sum_{t=1}^{N}(\mathrm{Obs}_t-X_t)^2}, \quad (12)$$

where N is the entire simulation period, Obs_t is the ground observation at time t, X_t is the simulated value at same time.

The simulated SM values at the Maqu Station by using these three methods are presented in Fig. 5a. The NO result shows few changes of SM throughout the entire simulation period and can't reflect the significant changes in actual SM, especially on 21 and 31 July. Although the temporal variation of estimated SM has been assimilated into the simulation by using DI method, the simulation result is inaccurate due to the low SM values estimated from AMSR-E, especially on 18–23 July. The temporal variation of estimated SM is also revealed in the simulation test by using the NR method, furthermore, the simulated SM not only reflects significant SM changes on 21 and 31 July, but also has less error than the DI result on 18–23 July. The RMSE values of NO, DI and NR results at this station are 0.07, 0.06 and 0.04 m^3/m^3, respectively, and the NR method is ranked the best estimation among all these three methods.

The SM simulation results at the Tanglha Station (Fig. 5b) are similar to that at the Maqu Station. The simulated SM values with NO method are much larger than the ground observations throughout the entire simulation period. The simulated SM values with DI method, however, are too small. The NR method could make the simulated SM values much close to the estimated SM values. Through the fine tuning of relaxation factor and quality factor, the evolution of simulated SM is close to that of the ground observations. The RMSE values of NO, DI and NR results at this station are 0.12, 0.07 and 0.05 m^3/m^3, respectively. Furthermore, the DI method, compared with the NR method, produces a larger concussion to the numerical model at temporal scale.

As a conclusion, the best simulating results are achieved by assimilating the estimated SM with the NR method. It makes the simulated SM tend to the ground observations step by step and the temporal characteristic of SM be disclosed. This is

helpful for numerical model to improve the simulating accuracy of SM in rainy events and seasonal variations.

6 Conclusion and discussion

In this paper, the potential by using satellite microwave bright temperature data to improve the performance of numerical simulations of SM has been analyzed. The SM estimated from AMSR-E is assimilated into the Noah land surface model by the NR method for the first time. The main conclusions are as follows:

1. The regional SM values have been estimated from AMSR-E brightness temperature data by the Yan et al. (2004)'s theory. The results show that the SM values estimated by this method are acceptable and the SM distributions are somewhat better than that from the AMSR-E daily SM product over the eastern part of the Qinghai-Tibet Plateau.

2. The temporal variations of the estimated SM are in good agreement with ground daily precipitations, though the estimated SM values are lower when compared with the Maqu Station and the Tanglha Station observational data and the NCEP reanalysis SM dataset.

3. Compared with the NO or DI method, the NR method shows a great advantage in simulation of SM variations. At regional scale, the simulated SM values are improved most in desert area, and then in grass, shrub and grass mixed zone. At temporal scale, the RMSE values between the simulated SM and the ground measured SM are decreased 0.03 and 0.07 m^3/m^3 by using the NR method in the Maqu Station and the Tanglha Station, respectively.

It is revealed from the above conclusions, a key factor in numerical assimilating simulations is to improve the accuracy of estimated SM values, that is, a good simulation

depends on high quality satellite remote sensing data to be assimilated into the land surface model.

In addition, there is a great concern about the direct insertion of estimated SM into numerical models. Ookouchi et al. (1984) mentioned that sharp horizontal SM gradients may generate thermal circulations as strong as sea breezes and thus may trigger convection. With considering the constraint of satellite scanning region, if the DI method is deployed to assimilate the estimated SM, this method will easily lead to sharp horizontal SM gradient between the estimated SM and the simulated SM at the intersection border. And this sharp horizontal gradient of SM has negative effect for the WRF model to simulate convection and make the model produce more fake precipitations near the intersection border. The NR method could weaken these sharp horizontal SM gradient through a period of nudging assimilation.

The shortcoming of NR method is that its parameter settings need an experience. It will be helpful to reduce the errors introduced from the estimated SM by developing better assimilate ways or even assimilating the satellite measured brightness temperature data directly.

Acknowledgements. This work is supported by the National Science Foundation of China (Grant No. 40775022) and the Innovation Project of the Chinese Academy of Sciences (KZCX2-YW-328) and the National Basic Research Program of China. The authors would like to thank the Tanglha Station and the Maqu Station of the Cold and Arid Regions Environmental and Engineering Research Institute, Chinese Academy of Sciences, for providing the soil moisture and precipitation datasets.

References

Chen, F. and Dudhia, J.: Coupling an advanced land-surface/hydrology model with the Penn State/NCAR MM5 modeling system, Part I: model description and implementation, Mon. Wea. Rev., 129(4), 569–585, 2001.

Clark, C. A. and Arritt, R. W.: Numerical simulations of the effect of soil moisture and vegetation cover on the development of deep convection, J. Appl. Meteor., 34, 2029–2045, 1995.

Cosby, B. J., Hornberger, G. M., Clapp, R. B., and Ginn, T. R.: A statistical exploration of the relationships of soil moisture characteristics to the physical properties of soils, Water Resour. Res., 20(6), 682–690, 1984.

Delworth, T. L. and Manabe, S.: The influence of potential evaporation on the variabilities of simulated soil wetness and climate, J. Climate, 1(5), 523–547, 1988.

Gallus Jr., W. A. and Segal, M.: Sensitivity of forecast rainfall in a Texas convective system to soil moisture and convective parameterization, Weather Forecast., 15, 509–525, 2000.

Gao, H., Wood, E. F., Jackson, T. J., and Drusch, M.: Using TRMM/TMI to retrieve surface soil moisture over the southern United States from 1998 to 2002, J. Hydrometeorol., 7(1), 23–38, 2006.

Gruhier, C., Rosnay, P. d., Kerr, Y., Mougin, E., Ceschia, E., Calvet, J.-C., and Richaume, P.: Evaluation of AMSR-E soil moisture product based on ground measurements over temperate and semi-arid regions, Geophys. Res. Lett., 35, L10405, doi:10410.11029/12008GL033330, 2008.

Hallikainen, M. T., Ulaby, F. T., Dobson, M. C., and El-Rayes, M. A.: Microwave dielectric behavior of wet soil-part 1: empirical models and experimental observations, IEEE T. Geosci. Remote., GE-23(1), 25–34, 1985.

Hoke, J. and Anthes, R.: The initialization of numerical models by a dynamic relaxation technique, Mon. Wea. Rev., 104, 1551–1556, 1976.

Huang, C., Li, X., Lu, L., and Gu, J.: Experiments of one-dimensional soil moisture assimilation system based on ensemble Kalman filter, Remote Sens. Environ., 112, 888–900, 2007.

Jackson, T. J., Hsu, A. Y., and O'Neill, P. E.: Surface soil moisture retrieval and mapping using high-frequency microwave satellite observation in the southern great plain, J. Hydrometeorol., 3, 688–699, 2002.

Jin, Y.-Q.: Monitoring regional sea ice of China's Bohai sea by SSM/I scattering indexes, IEEE J. Oceanic Eng., 23(2), 141–144, 1998.

Kistler, R. E.: A study of data assimilation techniques in an autobarotropic, primitive equation, channel model, M.S. thesis, Pennsylvania State University, 1974.
Lanicci, J. M., Carlson, T. N., and Warner, T. T.: Sensitivity of the Great Plains severe-storm environment to soil-moisture distribution, Mon. Wea. Rev., 115, 2660–2673, 1987.
McCabe, M. F., Gao, H., and Wood, E. F.: Evaluation of AMSR-E-Derived soil moisture retrievals using ground-based and PSR airborne data during SMEX02, J. Hydrometeorol., 6(6), 864–877, 2005a.
McCabe, M. F., Wood, E. F., and Gao, H.: Initial soil moisture retrievals from AMSR-E: multi-scale comparison using in situ data and rainfall patterns over Iowa, Geophys. Res. Lett., 32, L06403, doi:06410.01029/02004GL021222, 2005b.
Meesters, A. G. C. A., Jeu, R. A. M. D., and Owe, M.: Analytical derivation of the vegetation optical depth from the microwave polarization difference index, IEEE Geosci. Remote Sens. Lett., 2(2), 121–123, 2005.
Njoku, E. G. and Chan, S. K.: Vegetation and surface roughness effects on AMSR-E land observations, Remote Sens. Environ., 100(2), 190–199, 2006.
Njoku, E. G., Jackson, T. J., Lakshmi, V., Chan, T. K., and Nghiem, S. V.: Soil moisture retrieval from AMSR-E, IEEE Trans. Geosci. Remote Sens., 41(2), 215–229, 2003.
Ookouchi, Y., Segal, M., Kessler, R. C., and Piekle, R. A.: Evaluation of soil moisture effects on generation and modification of mesoscale circulations, Mon. Wea. Rev., 112, 2281–2292, 1984.
Prigent, C., Aires, F., Rossow, W. B., and Robock, A.: Sensitivity of satellite microwave and infrared observation to soil moisture at a global scale: relationship of satellite observations to in situ soil moisture measurements, J. Geophys. Res., 110, D07110, doi:07110.01029/02004JD005087, 2005.
Simonetta, P., Giovanni, M., and Emanuele, S.: Soil moisture estimates from AMSR-E brightness temperatures by using a dual-frequency algorithm, IEEE Trans. Geosci. Remote Sens., 44(11), 3135–3144, 2006.
Ulaby, F. T., Moore, R. K., and Fung, A. K.: Microwave Remote Sensing: Active and Passive, vol. 1, Microwave Remote Sensing Fundamentals and Radiometry, Addison-Wesley Publishing Co., Mass., p. 456, 1981
Vinnikov, K. Y., Robock, A., Qiu, S., and Entin, J. K.: Satellite remote sensing of soil moisture in Illinois, United States, J. Geophys. Res., 104(D4), 4145–4168, 1999.
Vinnikov, K. Y. and Yeserkepova, I. B.: Soil moisture: empirical data and model results, J.

Climate, 4(1), 66–79, 1991.
Wagner, W., Scipal, K., Pathe, C., Gerten, D., Lucht, W., and Rudolf, B.: Evaluation of the agreement between the first global remotely sensed soil moisture data with model and precipitation data, J. Geophys. Res., 108(D19), 4611, doi:4610.1029/2003JD003663, 2003.
Wang, L., Li, Z., and Chen, Q.: New calibration method for soil roughness parameters with AMSR-E observations, Chin. J. Remote Sens., 10(10), 654–660, 2006.
Wei, M.-Y.: Soil moisture: Report of a workshop held in Tiburon, California, 25–27 Jan 1994, NASA Conf. Publ. 3319, p. 80, 1995.
Wen, J., Jackson, T. J., and Bindlish, R.: Retrieval of soil moisture and vegetation water content using SSM/I data over a corn and soybean region, J. Hydrometeorol., 6(6), 854–863, 2005.
Wu, G.-X., Liu, Y.-M., Liu, X., Duan, A.-M., and Liang, X.-Y.: How the heating over the Tibetan plateau affects the asian climate in summer, Chin. J. Atmos. Sci., 29(1), 47–56, 2005.
Yan, F.-H. and Jin, Y.-Q.: Statistics of the average distance of polarization index derived from data of space-borne microwave remote sensing and soil moisture mapping, Chin. J. Radio Sci., 19(4), 386–392, 2004.

Table 1. Empirical coefficients of real and imaginary parts of soil dielectric constant at 6.9 GHz.

6.9 GHz	a_0	a_1	a_2	b_0	b_1	b_2	c_0	c_1	c_2
Real part	1.993	0.002	0.015	38.086	−0.176	−0.633	10.720	1.256	1.522
Imaginary part	−0.123	0.002	0.003	7.502	−0.058	−0.116	2.942	0.452	0.543

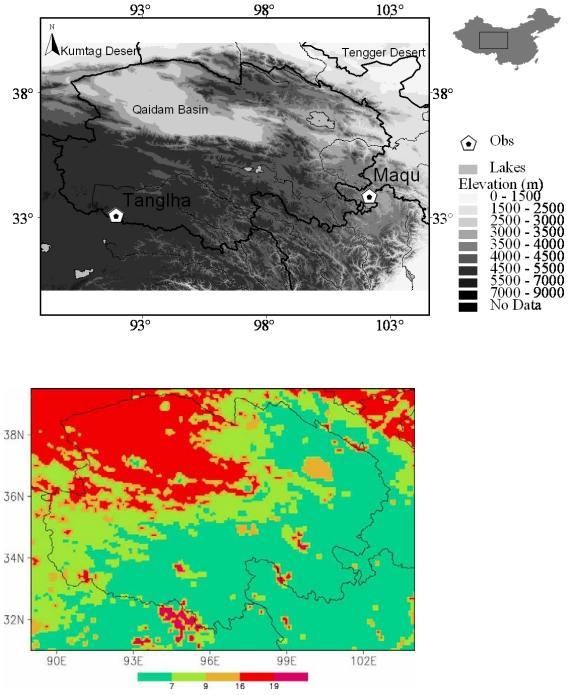

Fig. 1. Map of the digital elevation model and the observation sites **(a)**, and the distribution of land use classification **(b)** (where, 7 is grassland, 9 is mixed shrubland/grassland, 16 is water body, and 19 is barren or sparsely vegetated land) in the study area.

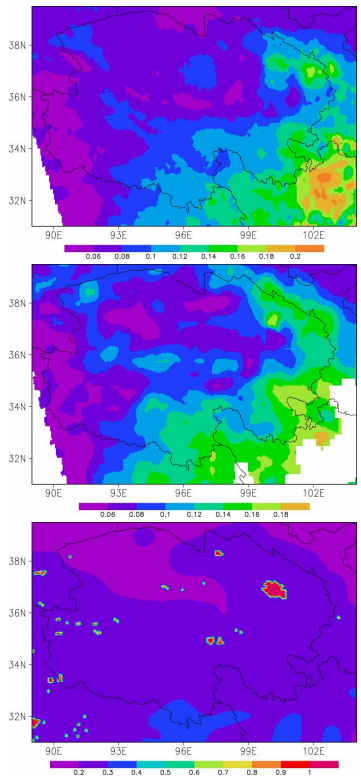

Fig. 2. The regional distributions of the AMSR-E derived SM **(a)**, the daily AMSR-E SM product **(b)**, and the NCEP SM at a 0–10 cm depth **(c)** at 14:00 BST 7 July 2008.

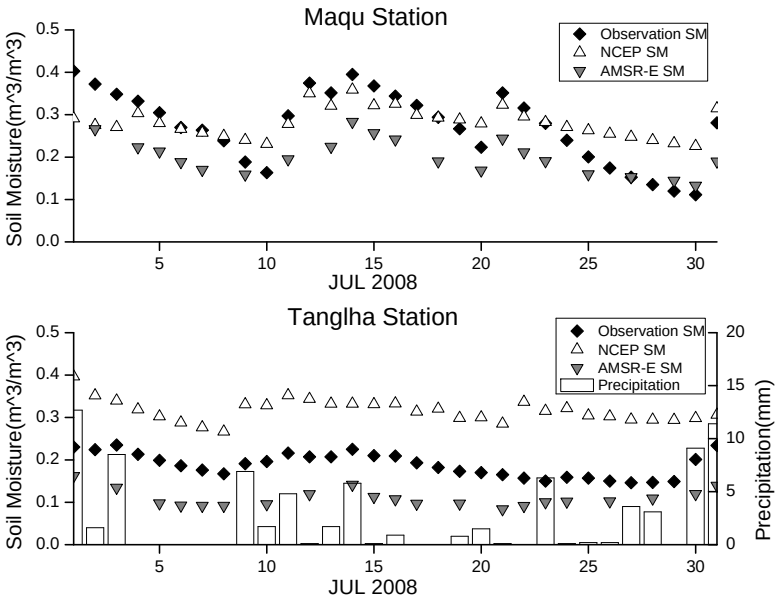

Fig. 3. The temporal variations of the AMSR-E derived SM, the NCEP SM at 0–10 cm depth and the field observations at 5 cm depth in the Maqu Station **(a)** and the Tanglha Station **(b)** at 14:00 BST July 2008.

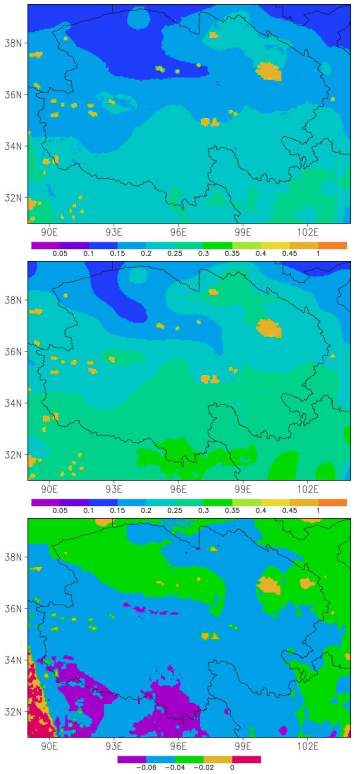

Fig. 4. The regional distributions of the simulated SM with assimilation **(a)**, non-assimilation **(b)**, and their discrepancy **(c)** at 14:00 BST 7 July 2008.

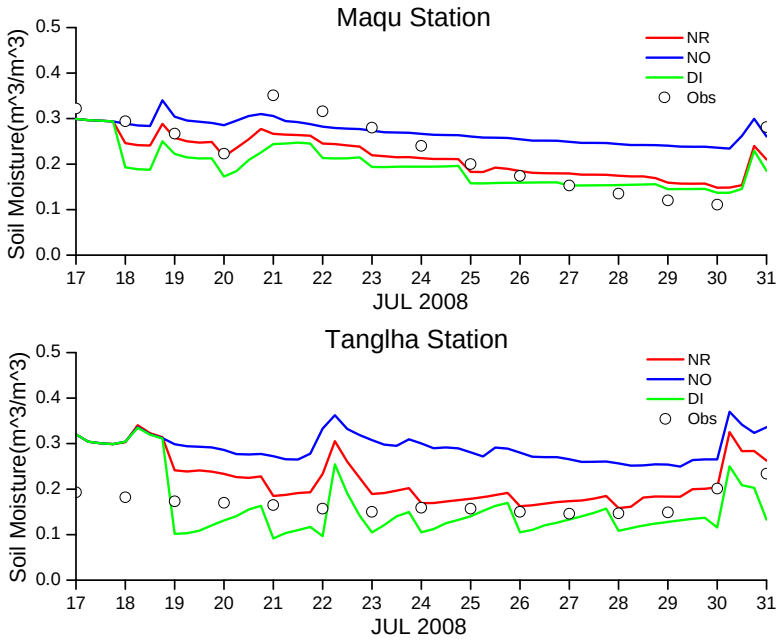

Fig. 5. The evolutions of the ground observations and the simulated SMs in the Maqu Station **(a)** and the Tanglha Station **(b)** from 17 to 31 July, 2008.